

Taylor's swimming sheet in a smectic-*A* liquid crystal

Harsh Soni 

School of Physical Sciences, IIT Mandi, Kamand, Mandi, Himachal Pradesh 175005, India



(Received 8 February 2023; accepted 26 April 2023; published 15 May 2023)

We calculate the swimming speed of a Taylor sheet in a smectic-*A* liquid crystal. Assuming that the amplitude of the wave propagating on the sheet is much smaller than the wave number, we solve the governing equations using the method of series expansion up to the second order in amplitude. We find that the sheet can swim much faster in smectic-*A* liquid crystals than in Newtonian fluids. The elasticity associated with the layer compressibility is responsible for the enhanced speed. We also calculate the power dissipated in the fluid and the flux of the fluid. The fluid is pumped opposite to the direction of the wave propagation.

DOI: [10.1103/PhysRevE.107.055104](https://doi.org/10.1103/PhysRevE.107.055104)

I. INTRODUCTION

The motility of microorganisms strongly depends on the dynamical properties of the surrounding fluid [1]. In this context, recent studies have focused on the following properties of fluids: shear-dependent viscosity, viscoelasticity, anisotropy, activity, etc. [2–9]. The purpose of this paper is to advance the understanding of microswimming in anisotropic media. Powers and co-workers have conducted notable research in this direction: The swimming dynamics of microorganisms in hexatic and nematic liquid crystals is now well understood [5–7,9].

In this work we ask how the motility of microorganisms is affected when the ambient fluid breaks the rotational and the translational symmetries together. The smectic liquid crystal is an example of a system with such a scenario [10], in which the elongated molecules not only are aligned in one direction, but are also arranged in layers, thus breaking the translational symmetry as well. Within a layer, smectics show fluidlike properties, whereas, normal to the layers, the elasticity emerges due to the broken translational symmetry. Moreover, they are known for showing striking dynamical properties such as diverging viscosity coefficients at low frequencies [11,12]. We study here the swimming microorganisms in smectic-*A* liquid crystals which have the molecules aligned along the direction normal to the layers [10].

To some extent, the nematic order has been seen in biological fluids [13–15], but no example of the microorganisms inhabiting smectic media is known so far. However, the microswimming in anisotropic media is not studied only in this context; another motivation stems from the use of liquid crystals as a medium for biomedical and biological sensing applications [16–18]. Furthermore, microswimmers in liquid crystals also have applications in cargo transport and microfluidics [19]. In addition, the suspension of microorganisms in a liquid crystal, known as a living liquid crystal, has seen remarkable progress recently, because it enables controlled experimental studies of active systems [20–22]. In such systems, mobility is crucial as it describes the ability of the microorganism to convert its biological energy into work that drives the system away from equilibrium. The motility of

bacteria has been studied in nematic liquid crystals [23–26], but no experiments have yet been performed with microorganisms in smectic liquid crystals. On the theoretical side, the dynamics of a single microswimmer in a smectic liquid crystal has been studied using a stochastic model [27].

To estimate the swimming speed of microorganisms, we use a simple model introduced by Taylor, namely, a two-dimensional sheet waving with a propagating wave of the displacement normal to the sheet [28]. As usual, we work with the assumption that the wave amplitude is small enough such that one can take advantage of the method of series expansion. The main result of this paper is that the swimming speed of the Taylor sheet is remarkably high in smectic-*A* liquid crystals when it is aligned parallel to the smectic layers. It is found to be proportional to the layer compressibility elastic constant. We also calculate the power dissipated and the flux of the fluid pumped by the sheet; the fluid is pumped opposite to the direction of the wave propagation. The sheet cannot swim through the smectic-*A* liquid crystal if it is tilted with respect to the smectic layers.

The rest of the paper is arranged as follows. In Sec. II we discuss the setup of the problem. In Sec. III the series expansion method implemented to solve the problem is described. In Sec. IV the results are presented. We conclude with a discussion and a summary in Sec. V.

II. SETUP

This section is organized in the following manner. In Sec. II A we review the theory of smectic-*A* liquid crystals. We then talk about the Taylor sheet in Sec. II B and the boundary conditions in Sec. II C. In Sec. II D the experimental values of various parameters are stated.

A. Theory of smectic-*A* liquid crystals

As discussed earlier, due to the layered arrangement of the molecules (see Fig. 1), smectic-*A* liquid crystals break translational symmetry, which gives rise to another hydrodynamic or slow variable, namely, the displacement field $u(\mathbf{r})$: A material point \mathbf{r} of the deformed smectic-*A* liquid crystal

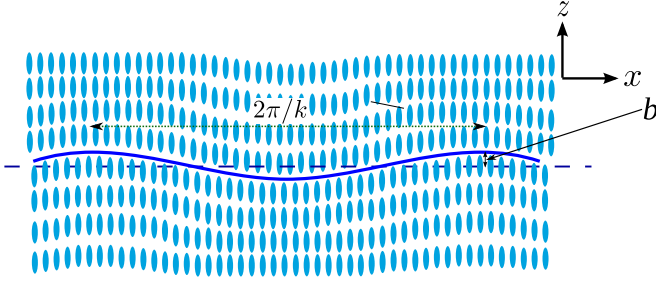


FIG. 1. (a) Schematic diagram of a Taylor sheet in a smectic-A liquid crystal. The ellipses represent the smectic molecules. The sheet is subject to a propagating wave of wave number k , amplitude b , and angular frequency ω .

was at the position $\mathbf{r} - u(\mathbf{r})\mathbf{n}_0$ before deformation, where \mathbf{n}_0 is the direction of the alignment of the undeformed smectic-A liquid crystal. The free-energy density for the smectic-A liquid crystal reads [10,12,29,30]

$$f(u) = \frac{1}{2}[BE^2 + K(\nabla^2 u)^2], \quad (1)$$

where

$$E = \nabla_{\parallel} u - \frac{1}{2}(\nabla u)^2, \quad (2)$$

$\nabla_{\parallel} \equiv \mathbf{n}_0 \cdot \nabla$, and B and K are the layer compressibility elastic constant and the Frank constant for splay deformations or the layer bending stiffness, respectively. Here we have ignored $(\nabla_{\parallel}^2 u)^2$ and $\nabla_{\parallel}^2 u \nabla_{\perp}^2 u$ terms ($\nabla_{\perp}^2 \equiv \nabla^2 - \nabla_{\parallel}^2$) for the following two reasons: (i) They are negligible and undetectable [10,29] and (ii) if they are included, the force per unit volume on the fluid due to the elasticity of the smectic-A liquid crystal cannot be written as the divergence of a stress tensor. The equations of motion for u and the velocity field \mathbf{v} for an incompressible smectic-A fluid of mass density ρ are given by [10–12,29,31]

$$\frac{\partial u}{\partial t} + \mathbf{v} \cdot \nabla u = \mathbf{n}_0 \cdot \mathbf{v} - \xi \frac{\delta F}{\delta u}, \quad (3a)$$

$$\rho \left(\frac{\partial \mathbf{v}}{\partial t} + (\mathbf{v} \cdot \nabla) \mathbf{v} \right) = \nabla \cdot \boldsymbol{\sigma}^v \mathbb{T} - \nabla p - \mathbf{w} \frac{\delta F}{\delta u}, \quad (3b)$$

$$\nabla \cdot \mathbf{v} = 0, \quad (3c)$$

where superscript \mathbb{T} stands for the transpose,

$$F[u] = \int d^3x f(u) \quad (4)$$

is the free-energy functional for the smectic-A liquid crystal,

$$\boldsymbol{\sigma}^v = \eta(\nabla \mathbf{v} + \nabla \mathbf{v}^{\mathbb{T}}) \quad (5)$$

is the viscous stress tensor,

$$\mathbf{w} = \frac{\partial E}{\partial(\nabla u)} = \mathbf{n}_0 - \nabla u, \quad (6)$$

p is the pressure, η is the kinetic viscosity, and ξ is the permeation coefficient. The vector $\mathbf{w}(\mathbf{r})$ gives the direction normal to the smectic layer at position \mathbf{r} [32]. As can be seen from Eq. (3a), the local velocity of the smectic layer is different from the local fluid velocity, so the fluid can pass through the layers, that is, the layers are permeable to the fluid [33]. The permeation coefficient ξ quantifies

this permeability. The field $-\delta F/\delta u$ in Eq. (3a) tries to restore the undeformed smectic. Equation (3c) is nothing but a continuity equation when the density is uniform. In general, smectic-A liquid crystals exhibit anisotropic viscous behavior [31], which has been disregarded here since we already have many parameters in the problem. Anyway, the anisotropy in the viscosity does not play a crucial role in the story presented here (see Sec. IV). The last term in Eq. (3b) is the force per unit volume on the fluid due to the elasticity owing to the broken translational symmetry along \mathbf{n}_0 . As our system is momentum conserving, one should be able to write this term as the divergence of a stress tensor as in

$$-\mathbf{w} \frac{\delta F}{\delta u} = \nabla \cdot \boldsymbol{\sigma}^e \mathbb{T}. \quad (7)$$

Indeed, this is possible for the free-energy density given by Eq. (1) with the expression of the elastic or reactive stress tensor $\boldsymbol{\sigma}^e$ [12,32],

$$\sigma_{ij}^e = \delta_{ij} f + w_i h_j + \frac{\partial f}{\partial(\nabla^2 u)} \partial_j w_i, \quad (8)$$

where

$$h_i = \frac{\delta F}{\delta(\partial_i u)} = \frac{\partial f}{\partial(\partial_i u)} - \partial_i \frac{\partial f}{\partial(\nabla^2 u)}. \quad (9)$$

Note that σ_{ij}^e is not symmetric. However, the law of conservation of the angular momentum demands that it should be symmetric [31]. One can easily symmetrize it when f is quadratic in ∇u , which is our case [12]; the symmetric form of σ_{ij}^e is given by

$$\begin{aligned} \sigma_{ij}^e &= \delta_{ij} \left[f + \partial_k \left(w_k \frac{\partial f}{\partial(\nabla^2 u)} \right) \right] + w_i h_j - w_j \partial_i \frac{\partial f}{\partial(\nabla^2 u)} \\ &= \delta_{ij} \left[f + \partial_k \left(w_k \frac{\partial f}{\partial(\nabla^2 u)} \right) \right] + w_i \frac{\partial f}{\partial(\partial_j u)} \\ &\quad - \left(w_j \partial_i \frac{\partial f}{\partial(\nabla^2 u)} + w_i \partial_j \frac{\partial f}{\partial(\nabla^2 u)} \right). \end{aligned}$$

The symmetric nature of the above σ_{ij}^e is obvious since

$$\frac{\partial f}{\partial(\partial_j u)} = B E w_j. \quad (10)$$

The net stress tensor then reads

$$\boldsymbol{\sigma} = \boldsymbol{\sigma}^v + \boldsymbol{\sigma}^e - \mathbf{I}p. \quad (11)$$

Then the right-hand side of Eq. (3b) is $\nabla \cdot \boldsymbol{\sigma}^{\mathbb{T}}$. The elastic stress $\boldsymbol{\sigma}^e$ is not uniquely defined [10], although that is not a matter of concern since our final results are independent of the choice of $\boldsymbol{\sigma}^e$ (see Appendix A). As microorganisms swim at low Reynolds number, we drop the terms on the left-hand side of Eq. (3b). Then, after rearranging their terms, Eqs. (3a) and (3b) reduce to

$$\frac{1}{\xi} \left(\frac{\partial u}{\partial t} + \mathbf{v} \cdot \nabla u - \mathbf{n}_0 \cdot \mathbf{v} \right) = B \nabla \cdot (E \mathbf{w}) - K \nabla^4 u, \quad (12a)$$

$$\mathbf{w} [B \nabla \cdot (E \mathbf{w}) - K \nabla^4 u] = -\eta \nabla^2 \mathbf{v} + \nabla p. \quad (12b)$$

B. Taylor sheet

We consider a Taylor sheet in the xy plane which is undulating with a propagating wave of the height function $Z(x, t) = b \sin(kx - \omega t)$, where b , k , and ω are the amplitude, wave number, and angular frequency of the wave, respectively. The speed of the wave is $c = \omega/k$. Assuming that the smectic layers are parallel to the plane of the sheet, i.e., $\mathbf{n}_0 = \hat{\mathbf{z}}$ (see Fig. 1), when the sheet is tilted with respect the smectic layers, it is unable to swim (see Appendix B). We further restrict ourselves to the regime of $\epsilon = bk \ll 1$.

C. Boundary conditions

We obtain the solution of Eqs. (12) in the $z \geq Z(x, t)$ region in a coordinate frame comoving with the sheet; solving the problem for the other side of the sheet yields the same results. We enforce the no-slip boundary condition on the sheet. Therefore, the fluid velocity at $z = Z(x, t)$ is simply given by $\hat{\mathbf{z}}\dot{Z}$, that is,

$$\mathbf{v}(z = Z) = \hat{\mathbf{z}}\dot{Z} = -\hat{\mathbf{z}}c\epsilon \cos(kx - \omega t). \quad (13)$$

We also consider that the smectic layers adjacent to the sheet are anchored to it, which gives us the following boundary condition on u :

$$u(z = Z) = Z(x, t) = \frac{1}{k} \sin(kx - \omega t). \quad (14)$$

Further, we assume that the surface of the sheet exerts no anchoring torque on the smectic molecules. The angle of the director of the deformed smectic with $\mathbf{n}_0 \equiv \hat{\mathbf{z}}$ is $\theta \simeq -\partial u/\partial x$. Then, at a point on the sheet [7,10],

$$K\mathbf{s} \cdot \nabla\theta \simeq -K\mathbf{s} \cdot \nabla \frac{\partial u}{\partial x} = 0, \quad (15)$$

where \mathbf{s} is the unit vector normal (pointing outward) to the sheet.

D. Various length scales and timescales and their experimental values

The smectic-A fluid has two length scales $(K/B)^{1/2}$ and $(\eta\xi)^{1/2}$ and a timescale η/B . The undulating sheet provides another length scale $1/k$ and timescale $1/\omega$. Therefore, in scaled units, only three dimensionless parameters can be varied independently; we choose to work with the parameters $K_s = Kk^2/\eta\omega$, $\xi_s = \eta\xi k^2$, and $B_s = B/\eta\omega$. Note that K_s is equivalent to the inverse of the Eriksen number [34]. The parameters K_s and B_s tell about the effects the bending stiffness and compressibility of the layers on the dynamics of the fluid, respectively, whereas ξ_s measures the comparative strengths of the following two forces on the fluid: the viscous force and the force due to the fluid motion relative to the smectic layers. For the microorganisms, $\omega \sim 1-10^2 \text{ s}^{-1}$ and $k \sim 10^4-10^5 \text{ cm}^{-1}$ [35], and for smectic-A liquid crystals, $B \sim 10^7-10^9 \text{ dyn/cm}^2$, $K \sim 10^{-7}-10^{-6} \text{ dyn}$, $\eta \sim 10^{-1}-1 \text{ P}$, and $\xi \sim 10^{-14} \text{ P}^{-1} \text{ cm}^2$ [10,12,36-39]. Then $K_s \sim 10^{-1}-10^5$, $B_s \sim 10^5-10^{10}$, $\xi_s \sim 10^{-7}-10^{-4}$, $K_s/B_s \sim 10^{-8}-10^{-3}$, and $B_s\xi_s \sim 10^{-1}-10^3$; thus $\xi_s \ll 1$, $B_s \gg 1$, and $K_s \ll B_s$.

III. SOLUTION USING SERIES EXPANSION METHOD

As the fluid is considered to be incompressible [see Eq. (3c)], the velocity field can be written as the curl of a stream function $\hat{\mathbf{y}}\psi(x, z)$:

$$\mathbf{v} = \nabla \times [\hat{\mathbf{y}}\psi(x, z)]. \quad (16)$$

The series expansions for the variables u , ψ , and p in ϵ have the form

$$\phi = \epsilon\phi^{(1)} + \epsilon^2\phi^{(2)} + \dots \quad (17)$$

The ϵ terms of Eqs. (12) then give

$$\frac{1}{\xi} \left(\frac{\partial u^{(1)}}{\partial t} - \frac{\partial \psi^{(1)}}{\partial x} \right) - B \frac{\partial^2 u^{(1)}}{\partial z^2} + K \nabla^4 u^{(1)} = 0, \quad (18a)$$

$$-B \frac{\partial^3 u^{(1)}}{\partial z^2 \partial x} + K \nabla^4 \left(\frac{\partial u^{(1)}}{\partial x} \right) + \eta \nabla^4 \psi^{(1)} = 0. \quad (18b)$$

Equation (18b) is obtained by taking the curl of Eq. (12b). We solve the above equations with the boundary conditions given by the leading-order expressions of Eqs. (13)–(15),

$$\left. \frac{\partial \psi^{(1)}}{\partial z} \right|_{z=0} = 0, \quad (19a)$$

$$\left. \frac{\partial \psi^{(1)}}{\partial x} \right|_{z=0} = -c \cos(kx - \omega t), \quad (19b)$$

$$u^{(1)}|_{z=0} = \frac{1}{k} \sin(kx - \omega t), \quad (19c)$$

$$\left. \frac{\partial^2 u^{(1)}}{\partial z \partial x} \right|_{z=0} = 0. \quad (19d)$$

That results in

$$u^{(1)} = \text{Re} \left[\left(\sum_{i=1}^4 A_i \exp(\alpha_i z) \right) \exp[i(kx - \omega t)] \right], \quad (20)$$

where α_i are the roots of the characteristic equation with $\text{Re}(\alpha_i) < 0$,

$$\left(\frac{\alpha}{k} \right)^8 + L_1 \left(\frac{\alpha}{k} \right)^6 + L_2 \left(\frac{\alpha}{k} \right)^4 + L_3 \left(\frac{\alpha}{k} \right)^2 + L_4 = 0, \quad (21)$$

where

$$L_1 = -4 - \frac{B_s}{K_s}, \quad (22a)$$

$$L_2 = \left(\frac{2B_s}{K_s} + 6 + \frac{1}{\xi_s} \right) - i \frac{1}{\xi_s K_s}, \quad (22b)$$

$$L_3 = \frac{2}{\xi_s K_s} i - \left(\frac{B_s}{K_s} + 4 + \frac{2}{\xi_s} \right) - \frac{B_s}{\xi_s K_s}, \quad (22c)$$

$$L_4 = 1 + \frac{1}{\xi_s} - i \frac{1}{\xi_s K_s}. \quad (22d)$$

The constants A_i are calculated using the boundary conditions (19). The expression of $\psi^{(1)}$ is readily obtained by integrating Eq. (18a) with respect to x , with the integration constant being zero; the value of the integration constant is redundant here since it does not contribute to the fluid velocity calculated using the curl of $\psi^{(1)}\hat{\mathbf{y}}$ [see Eq. (16)]. The terms with $\text{Re}(\alpha_i) > 0$ are discarded as they will lead to the divergence of the velocity field $\mathbf{v}^{(1)}$ at $z \rightarrow \infty$. Far from the sheet,

$\mathbf{v}^{(1)}$ vanishes, so the first-order speed of the sheet is zero. The second-order fields $u^{(2)}$, $\psi^{(2)}$, and $p^{(2)}$ have the following form:

$$\phi^{(2)} = \phi_0^{(2)}(z) + \text{Re}\{\phi_2^{(2)}(z) \exp[2i(kx - \omega t)]\}. \quad (23)$$

Therefore, their time-averaged values are independent of x . Then time averaging the ϵ^2 term of the x component of Eq. (12b) yields

$$\eta \frac{d^2}{dz^2} \langle v_x^{(2)} \rangle = \left\langle \frac{\partial u^{(1)}}{\partial x} \left(B \frac{\partial^2 u^{(1)}}{\partial z^2} - K \nabla^4 u^{(1)} \right) \right\rangle. \quad (24)$$

From Eq. (13), the boundary condition on $\langle v_x^{(2)} \rangle$ is

$$\langle v_x^{(2)} \rangle \Big|_{z=0} = -\frac{1}{k} \left\langle \frac{\partial v_x^{(1)}}{\partial z} \sin(kx - \omega t) \right\rangle \Big|_{z=0}. \quad (25)$$

Once we have the expressions of $u^{(1)}$ and $v_x^{(1)}$, it is straightforward to solve Eq. (24) with the above condition. As our calculation is performed in a frame moving with the velocity of the sheet, in the laboratory frame, the component of the velocity of the sheet along $-\hat{\mathbf{x}}$ is given by

$$U \simeq \langle v_x^{(2)} \rangle \Big|_{z \rightarrow \infty} \epsilon^2. \quad (26)$$

As seen in earlier studies, the Taylor sheet does not simply swim through liquid crystals; it also pumps the fluid [5,7]. In the laboratory frame, the time-averaged fluid flux in the x

direction is [5]

$$Q = \int_{Z(x,t)}^{\infty} dz [\langle v_x \rangle - U] \simeq \int_0^{\infty} dz [\epsilon^2 \langle v_x^{(2)} \rangle - U], \quad (27)$$

where $O(\epsilon^3)$ terms have been ignored.

We also measure the power dissipated per unit sheet area in the fluid using the formula [5]

$$\mathcal{P} = \frac{k}{2\pi} \int_{Z(x,t)}^{\infty} dz \int_{-\pi/k}^{\pi/k} dx [\sigma_{ij}^v (\partial_i v_j) + \xi (\nabla \cdot \mathbf{h})^2]. \quad (28)$$

The second term here measures the dissipation due the dissipative dynamics of u . The above expression is for the dissipation on one side (in $z \geq Z$ region) of the sheet; the total power dissipated would be twice its value. We calculate the leading-order term of \mathcal{P} which is quadratic in ϵ .

IV. RESULTS

As discussed in Sec. II B, for a typical microorganism in smectic- A liquid crystals, $\xi_s \ll 1$, $K_s \ll B_s$, and $B_s \gg 1$. In this case, one root of Eq. (21) is $\alpha_1 \simeq -k(B_s/K_s)^{1/2}$, which is much larger than k . It indicates the existence of a thin boundary layer of thickness of approximately $(K_s/B_s)^{1/2}/k \equiv (K/B)^{1/2}$ near the sheet, where the magnitude of the surface torque [10] $-K\hat{\mathbf{z}} \cdot \nabla(\partial u/\partial x)$ increases sharply with z from zero at the sheet [see the boundary condition (15)] and then slowly decreases beyond the boundary layer, recalling that the angle of the local smectic director with the z axis is $\theta \simeq -\partial u/\partial x$. This boundary layer is observed because the wavelength $2\pi/k$ is much larger than the characteristic length $(K/B)^{1/2}$ of the smectic. Another two roots are

$$\alpha_{2,3} \simeq -k \left(1 + \frac{K_s}{2B_s \xi_s} - i \frac{1}{2B_s \xi_s} \left\{ 1 \pm [4B_s^2 \xi_s - (i - K_s)^2]^{1/2} \right\} \right)^{1/2},$$

so $|\alpha_{2,3}| \gtrsim k$. The last root is $\alpha_4 = \alpha_r + i\alpha_i$, where

$$\alpha_r \simeq -k \left(\frac{K_s + \sqrt{1 + K_s^2}}{2B_s} \right)^{1/2}, \quad (29)$$

$$\alpha_i \simeq k \left(\frac{1}{2B_s(K_s + \sqrt{1 + K_s^2})} \right)^{1/2}. \quad (30)$$

Clearly, $|\alpha_4| \ll k$. Thus, α_4 is much smaller than the other three roots, and the leading-order solution of Eqs. (18) corresponds to this root only. The real part α_r of α_4 gives rise to the decay of $u^{(1)}$ and $\psi^{(1)}$, whereas the imaginary part α_i is responsible for the oscillatory behavior of these functions in the z direction. The approximate solution of Eqs. (18) is

$$u^{(1)} \simeq \frac{1}{k} \exp(-\alpha_r z) \sin(kx + \alpha_i z - \omega t), \quad (31)$$

$$\psi^{(1)} \simeq -\frac{c}{k} \exp(-\alpha_r z) \sin(kx + \alpha_i z - \omega t). \quad (32)$$

Note that $u^{(1)}$ and $\psi^{(1)}$ decay slowly with the distance from the sheet. The swimming speed of the sheet calculated as

discussed in the preceding section is given by

$$U \simeq \frac{1}{4} \frac{B_s}{K_s + \sqrt{1 + K_s^2}} c \epsilon^2 = \frac{1}{4} \frac{B}{\eta(K_s + \sqrt{1 + K_s^2})} k \epsilon^2. \quad (33)$$

Since $B_s \gg K_s$ and $B_s \gg 1$, U is much larger than the swimming speed of the Taylor sheet $U_N = c\epsilon^2/2$ in a Newtonian fluid. Moreover, U is independent of ω for $K_s \ll 1$. However, is the expression (33) of U approximately correct for all $\epsilon \ll 1$? To answer this question, we do a simple analysis to know the dependence of the fourth-order speed of the sheet U_4 on B_s and we find that U_4 goes as $\epsilon^4 B_s^n$, where n is a number which is definitely greater than 2 (see Appendix C). Hence our calculation is reasonable only when $B_s^{n-1} \epsilon^2 \ll 1$. Of course, this is not practical even if we consider that $n = 2$, because $B_s \gtrsim 10^5$. Nevertheless, our analysis hints that the smectic ordering may lead to a large enhancement in the swimming speed of the sheet.

Using Eq. (28), we get the following formula of the power dissipated per area of the sheet:

$$\mathcal{P} \simeq \left(\frac{B_s}{8(K_s + \sqrt{1 + K_s^2})} \right)^{1/2} \eta \omega c \epsilon^2. \quad (34)$$

Again, the power dissipated is also much larger than in the Newtonian case. The flux of the fluid is given by

$$Q \simeq -\frac{1}{2} \left(\frac{B_s}{2(K_s + \sqrt{1 + K_s^2})} \right)^{3/2} \frac{c}{k} \epsilon^2. \quad (35)$$

As $Q < 0$, the fluid is pumped opposite to the direction of the wave propagation.

We now briefly discuss the effect of the viscosity anisotropy. Adding the anisotropic part σ^{ani} to the viscous stress, we get

$$\sigma^v = \eta(\nabla \mathbf{v} + \nabla \mathbf{v}^T) + \sigma^{\text{ani}}. \quad (36)$$

For our quasi-two-dimensional system, $\sigma_{11}^{\text{ani}} = 2\Delta\eta_1\partial_1v_1$, $\sigma_{33}^{\text{ani}} = 2\Delta\eta_3\partial_3v_3$, and all other elements of σ^{ani} are zero [36]. The values of the coefficients $\Delta\eta_1$ and $\Delta\eta_3$ are of the order of η [12]. Then our approximate results given by Eqs. (33)–(35) remain unchanged. This is because the effect of the layer compressibility on the dynamics of the fluid is much stronger than that of the viscosity, since the viscosity coefficients are negligibly small compared to B/ω .

For the sake of completeness, the behavior of U , \mathcal{P} , and Q over a wider range of B_s , K_s , and ξ_s is shown in Appendix D. Here is a summary of what we find: $Q < 0$ for all the parameters values we investigated, so the fluid is pumped in the direction opposite to the direction of the wave on the sheet. All these quantities U , \mathcal{P} , and $-Q$ increase with B_s and decrease with both K_s and ξ_s , except that $-Q$ rather increases with ξ_s for small K ($=10^{-2}$). In the following two cases, the values of U , \mathcal{P} , and Q tend to their values for the Newtonian case, $\omega k^{-1}\epsilon^2/2$, $\eta\omega^2k^{-1}\epsilon^2$, and 0, respectively: (a) in the $\xi\eta k^2 \rightarrow \infty$ limit, since Eqs. (12) reduce to Stokes equations in this limit, and (b) when $Kk^2/B \gg 1$, in which case the solution of Eqs. (18) reads

$$\psi^{(1)} \simeq -\omega u^{(1)}/k \simeq -\frac{c}{k}(1+kz)\exp(-kz)\sin(kx-\omega t), \quad (37)$$

with $\nabla^4\psi^{(1)} \simeq \nabla^4u^{(1)} \simeq 0$. Then the terms on the right-hand side of Eq. (24) are negligible and the Newtonian results prevail.

V. CONCLUSION

The anisotropy of the medium gives rise to significant variations in the swimming speed of the Taylor sheet [5–7,9]. In fact, for nematic liquid crystals, the speed of the sheet can be enhanced up to five times compared to Newtonian fluids at large values of the rotational viscosity [7]. Here the sheet fails to be propelled when it is tilted with respect to the smectic layers (see Appendix B). Otherwise, the swimming speed is dramatically much larger than its Newtonian value for the typical experimental values of the parameters B_s , ξ_s , and K_s . Such a large boost has also been observed in the case active fluids [8], although the active fluid supplies the energy to sheet in that case. Indeed, our findings are approximately correct only if $\epsilon^2 \ll B_s^{-m}$, where m is a number which is definitely greater than one; this condition seems to be far from the reality as $B_s \gg 1$. We have also presented the results for a wider parameter range, which could be applicable in the context of artificial microswimmers and smectic-A liquid

crystals consisting of micron-sized particles such as filamentous viruses [40].

A numerical study of this problem would be useful to see whether the Taylor sheet can really swim that fast even for the large values of ϵ . Also, it would be interesting to investigate the swimming microorganisms in smectic-A liquid crystals; the bacterial swimming has already been explored in nematic liquid crystals [20,23–26].

To summarize, to get an estimate of the swimming speed of microorganisms in smectic-A liquid crystals, we modeled them as a Taylor sheet. We predict that, in smectic-A liquid crystals, the microorganisms can swim much faster than in Newtonian fluids. The sheet also pumps the fluid in the direction opposite to the direction of the propagating wave. We further calculated the power dissipated, which again it turned out to be much larger than the power dissipated for the Newtonian case.

ACKNOWLEDGMENT

We acknowledge Sriram Ramaswamy for clarifying his work on smectic-A liquid crystals [12].

APPENDIX A: NONUNIQUENESS OF THE STRESS TENSOR

Recalling Eq. (3b),

$$\rho \left[\frac{\partial \mathbf{v}}{\partial t} + (\mathbf{v} \cdot \nabla) \mathbf{v} \right] = \nabla \cdot \sigma^T, \quad (A1)$$

where

$$\sigma = \sigma^v + \sigma^e - \mathbf{I}p \quad (A2)$$

is the net stress tensor. From Eq. (7)

$$-\mathbf{w} \frac{\delta F}{\delta u} = \nabla \cdot \sigma^e T. \quad (A3)$$

Let us consider two different forms of the elastic stress tensor, σ_a^e and σ_b^e . From the above equation

$$\nabla \cdot \sigma_a^e T = -\mathbf{w} \frac{\delta F}{\delta u}, \quad (A4)$$

$$\nabla \cdot \sigma_b^e T = -\mathbf{w} \frac{\delta F}{\delta u}. \quad (A5)$$

Hence

$$\nabla \cdot \sigma_a^e T = \nabla \cdot \sigma_b^e T. \quad (A6)$$

In the calculation discussed in this paper, the form of the stress tensor σ becomes important only when we apply the condition that the net force $\mathbf{F}_{\text{sheet}}$ on the Taylor sheet should be zero. The expression of $\mathbf{F}_{\text{sheet}}$ reads

$$\mathbf{F}_{\text{sheet}} = - \int_s \sigma \cdot d\mathbf{A}, \quad (A7)$$

where the subscript s stands for the surface integration on the sheet and the surface element $d\mathbf{A}$ is pointing outward. As we choose the exponentially decreasing solution in the z direction, σ vanishes at $z \rightarrow \infty$. Then, from the divergence theorem,

$$\mathbf{F}_{\text{sheet}} = - \int \nabla \cdot \sigma^T dV. \quad (A8)$$

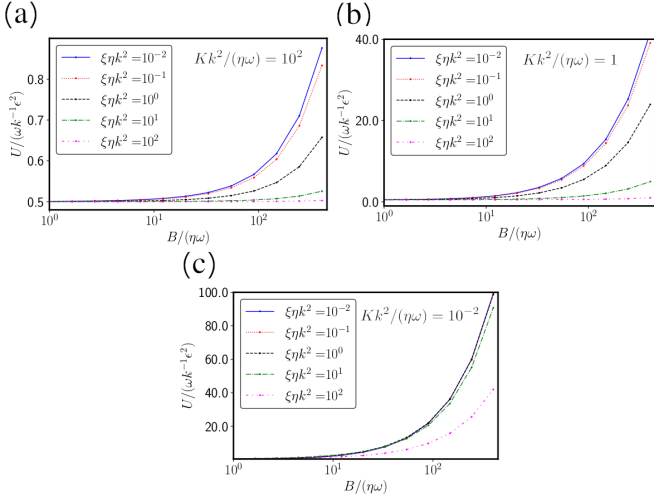


FIG. 2. Dependence of the scaled swimming speed $U/(\omega\epsilon^2/k)$ of a Taylor sheet on $B/\eta\omega$ for various values of $\xi\eta k^2$: (a) $Kk^2/\eta\omega = 10^2$, (b) $Kk^2/\eta\omega = 1$, and (c) $Kk^2/\eta\omega = 10^{-2}$.

For the two different forms of σ^e discussed above, the net forces on the sheet will be

$$\mathbf{F}_{\text{sheet}}^a = - \int \nabla \cdot (\boldsymbol{\sigma}^v + \boldsymbol{\sigma}_a^e - \mathbf{I}p)^\top dV, \quad (\text{A9})$$

$$\mathbf{F}_{\text{sheet}}^b = - \int \nabla \cdot (\boldsymbol{\sigma}^v + \boldsymbol{\sigma}_b^e - \mathbf{I}p)^\top dV. \quad (\text{A10})$$

Hence, from Eq. (A6),

$$\mathbf{F}_{\text{sheet}}^a - \mathbf{F}_{\text{sheet}}^b = - \int \nabla \cdot (\boldsymbol{\sigma}_a^e - \boldsymbol{\sigma}_b^e)^\top dV = 0. \quad (\text{A11})$$

So $\mathbf{F}_{\text{sheet}}^a = \mathbf{F}_{\text{sheet}}^b$, i.e., the net force on the sheet is independent of the form of the stress tensor chosen. Therefore, none of our results depend on the choice of the stress tensor.

APPENDIX B: SWIMMING SPEED OF A TAYLOR SHEET TILTED WITH RESPECT TO THE SMECTIC LAYERS

Let θ_0 be the angle of \mathbf{n}_0 with $\hat{\mathbf{z}}$; then $\mathbf{n}_0 = \sin\theta_0\hat{\mathbf{x}} + \cos\theta_0\hat{\mathbf{z}}$. Considering that $\theta_0 \neq 0$. The time average of the variables u , ψ , and p would be independent of x . Therefore, time averaging the n th-order term of Eq. (12) yields

$$\left(B \cos^2\theta_0 \frac{d^2}{dz^2} - K \frac{d^4}{dz^4} \right) \langle u^{(n)} \rangle = -\frac{1}{\xi} \sin\theta_0 \langle v_x^{(n)} \rangle + \Pi^{(n)}, \quad (\text{B1})$$

where all the n th-order nonlinear terms are buried in $\Pi^{(n)}$. Here n is a positive even integer; $\langle u^{(n)} \rangle$ and $\langle v^{(n)} \rangle$ vanish for the odd values of n . If the n th-order swimming speed of the sheet in the $-\hat{\mathbf{x}}$ direction is $U_n = U^{(n)}\epsilon^n$, then $v_x^{(n)}$ will have the form

$$\langle v_x^{(n)} \rangle = U^{(n)} + \langle \Delta v_x^{(n)} \rangle, \quad (\text{B2})$$

where $\langle \Delta v_x^{(n)} \rangle$ is the remaining part of $\langle v_x^{(n)} \rangle$, which exponentially decays to zero as $z \rightarrow \infty$. If $U^{(n)} \neq 0$, from Eq. (B1), $\langle u^{(n)} \rangle$ diverges at $z \rightarrow \infty$. Hence, $U^{(n)} = 0$ for all n . Therefore, if the sheeting is tilted with respect to the smectic layers, it cannot swim through the smectic-A liquid crystal.

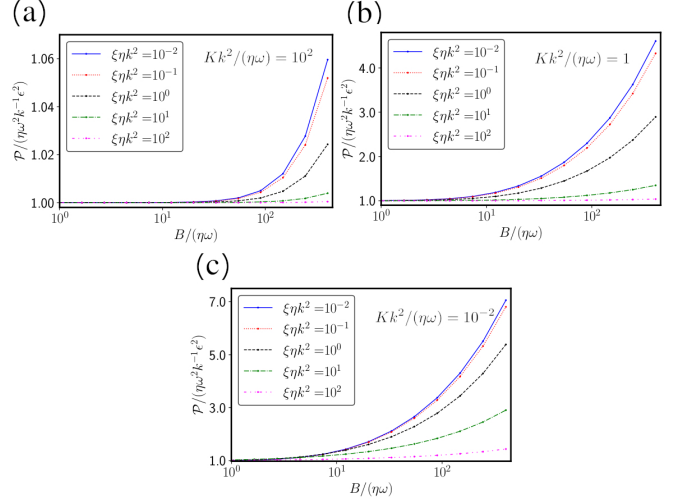


FIG. 3. Scaled power dissipated $\mathcal{P}/(\eta\omega^2\epsilon^2/k)$ in the smectic-A fluid as the function of $B/\eta\omega$ for different values of $\xi\eta k^2$: (a) $Kk^2/\eta\omega = 10^2$, (b) $Kk^2/\eta\omega = 1$, and (c) $Kk^2/\eta\omega = 10^{-2}$.

APPENDIX C: DEPENDENCE OF THE FOURTH-ORDER SPEED OF THE SHEET ON B_s

Averaging the fourth-order term of Eq. (12b) over time, we get

$$\eta \frac{d^2}{dz^2} \langle v_x^{(4)} \rangle = \frac{1}{2} B \left\langle \frac{\partial u^{(1)}}{\partial x} \nabla \cdot [\nabla u^{(1)} (\nabla u^{(1)})^2] \right\rangle + \Theta^{(4)}, \quad (\text{C1})$$

where $\Theta^{(4)}$ consists of all other nonlinear terms. For $\xi_s \ll 1$, $K_s \ll B_s$, and $B_s \gg 1$, $\nabla u^{(1)} \sim (k\hat{\mathbf{x}} + \alpha_r\hat{\mathbf{z}})u^{(1)}$ and $\alpha_r \ll k$, so the first term on the right-hand side of Eq. (C1) would be of

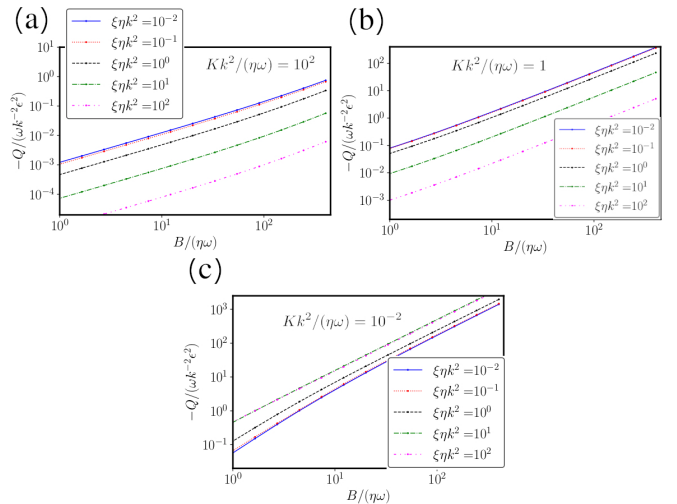


FIG. 4. Scaled flux $Q/(\omega\epsilon^2/k^2)$ of the fluid pumped by the Taylor sheet in the x direction as a function of $B/\eta\omega$ for different values of $\xi\eta k^2$: (a) $Kk^2/\eta\omega = 10^2$, (b) $Kk^2/\eta\omega = 1$, and (c) $Kk^2/\eta\omega = 10^{-2}$. Note that $Q < 0$. In contrast to the first two cases, $-Q$ increases with $\xi\eta k^2$ for $Kk^2/\eta\omega = 10^{-2}$.

the order of $Bk^5(u^{(1)})^4$. Hence, due to this term [see Eq. (31)],

$$\langle v_x^{(4)} \rangle \sim \frac{Bk}{\eta\alpha_r^2} \sim B_s c \frac{B_s}{K_s + \sqrt{1 + K_s^2}}. \quad (\text{C2})$$

As $\Theta^{(4)}$ may have the higher powers of B_s , one can say that the fourth-order swimming speed U_4 goes as $\epsilon^4 B_s^n$. Here we do not know the exact value of the number n , but it is certainly greater than 2.

APPENDIX D: RESULTS FOR A BROADER RANGE OF PARAMETERS

Figure 2 shows U vs B_s for the different values of K_s and ξ_s . Recall that $B_s \equiv B/\eta\omega$, $K_s \equiv Kk^2/\eta\omega$, and $\xi_s \equiv \xi\eta k^2$. How power dissipated in the fluid \mathcal{P} varies with B_s is shown in Fig. 3. The dependence of the flux Q of the fluid pumped by the sheet on B_s is displayed in Fig. 4.

-
- [1] S. E. Spagnolie and P. T. Underhill, Swimming in complex fluids, *Annu. Rev. Condens. Matter Phys.* **14**, 381 (2023).
- [2] C. Datt, L. Zhu, G. J. Elfring, and O. S. Pak, Squirming through shear-thinning fluids, *J. Fluid Mech.* **784**, R1 (2015).
- [3] D. Hewitt and N. Balmforth, Taylor's swimming sheet in a yield-stress fluid, *J. Fluid Mech.* **828**, 33 (2017).
- [4] E. Lauga, Propulsion in a viscoelastic fluid, *Phys. Fluids* **19**, 083104 (2007).
- [5] M. S. Krieger, S. E. Spagnolie, and T. R. Powers, Locomotion and transport in a hexatic liquid crystal, *Phys. Rev. E* **90**, 052503 (2014).
- [6] J. Shi and T. R. Powers, Swimming in an anisotropic fluid: How speed depends on alignment angle, *Phys. Rev. Fluids* **2**, 123102 (2017).
- [7] M. S. Krieger, S. E. Spagnolie, and T. R. Powers, Microscale locomotion in a nematic liquid crystal, *Soft Matter* **11**, 9115 (2015).
- [8] H. Soni, R. A. Pelcovits, and T. R. Powers, Enhancement of Microorganism Swimming Speed in Active Matter, *Phys. Rev. Lett.* **121**, 178002 (2018).
- [9] M. S. Krieger, S. E. Spagnolie, and T. R. Powers, Swimming with small and large amplitude waves in a confined liquid crystal, *J. Non-Newtonian Fluid Mech.* **273**, 104185 (2019).
- [10] P.-G. de Gennes and J. Prost, *The Physics of Liquid Crystals*, International Series of Monographs on Physics (Oxford University Press, Oxford, 1993), Vol. 83.
- [11] G. F. Mazenko, S. Ramaswamy, and J. Toner, Viscosities Diverge as $\frac{1}{\omega}$ in Smectic-A Liquid Crystals, *Phys. Rev. Lett.* **49**, 51 (1982).
- [12] G. F. Mazenko, S. Ramaswamy, and J. Toner, Breakdown of conventional hydrodynamics for smectic-A, hexatic-B, and cholesteric liquid crystals, *Phys. Rev. A* **28**, 1618 (1983).
- [13] C. Viney, A. E. Huber, and P. Verdugo, Liquid-crystalline order in mucus, *Macromolecules* **26**, 852 (1993).
- [14] I. I. Smalyukh, J. Butler, J. D. Shrout, M. R. Parsek, and G. C. L. Wong, Elasticity-mediated nematiclike bacterial organization in model extracellular dna matrix, *Phys. Rev. E* **78**, 030701(R) (2008).
- [15] F. C. Chrétien, Involvement of the glycoproteic meshwork of cervical mucus in the mechanism of sperm orientation, *Acta Obstet. Gyn. Scand.* **82**, 449 (2003).
- [16] C. J. Woolverton, E. Gustely, L. Li, and O. D. Lavrentovich, Liquid crystal effects on bacterial viability, *Liq. Cryst.* **32**, 417 (2005).
- [17] A. M. Lowe and N. L. Abbott, Liquid crystalline materials for biological applications, *Chem. Mater.* **24**, 746 (2012).
- [18] S. Shivanovskii, O. Lavrentovich, T. Schneider, T. Ishikawa, I. Smalyukh, C. Woolverton, G. Niehaus, and K. Doane, Lyotropic chromonic liquid crystals for biological sensing applications, *Mol. Cryst. Liq. Cryst.* **434**, 259/[587] (2005).
- [19] T. Turiv, R. Koizumi, K. Thijssen, M. M. Genkin, H. Yu, C. Peng, Q.-H. Wei, J. M. Yeomans, I. S. Aranson, A. Doostmohammadi *et al.*, Polar jets of swimming bacteria condensed by a patterned liquid crystal, *Nat. Phys.* **16**, 481 (2020).
- [20] S. Zhou, A. Sokolov, O. D. Lavrentovich, and I. S. Aranson, Living liquid crystals, *Proc. Natl. Acad. Sci. USA* **111**, 1265 (2014).
- [21] I. S. Aranson, Harnessing medium anisotropy to control active matter, *Acc. Chem. Res.* **51**, 3023 (2018).
- [22] N. Figueroa-Morales, M. M. Genkin, A. Sokolov, and I. S. Aranson, Non-symmetric pinning of topological defects in living liquid crystals, *Commun. Phys.* **5**, 301 (2022).
- [23] A. Kumar, T. Galstian, S. K. Pattanayek, and S. Rainville, The motility of bacteria in an anisotropic liquid environment, *Mol. Cryst. Liq. Cryst.* **574**, 33 (2013).
- [24] A. Sokolov, S. Zhou, O. D. Lavrentovich, and I. S. Aranson, Individual behavior and pairwise interactions between microswimmers in anisotropic liquid, *Phys. Rev. E* **91**, 013009 (2015).
- [25] S. Zhou, O. Tovkach, D. Golovaty, A. Sokolov, I. S. Aranson, and O. D. Lavrentovich, Dynamic states of swimming bacteria in a nematic liquid crystal cell with homeotropic alignment, *New J. Phys.* **19**, 055006 (2017).
- [26] M. Goral, E. Clement, T. Darnige, T. Lopez-Leon, and A. Lindner, Frustrated 'run and tumble' of swimming *Escherichia coli* bacteria in nematic liquid crystals, *Interface Focus* **12**, 20220039 (2022).
- [27] C. Ferreiro-Córdova, J. Toner, H. Löwen, and H. H. Wensink, Long-time anomalous swimmer diffusion in smectic liquid crystals, *Phys. Rev. E* **97**, 062606 (2018).
- [28] G. Taylor, Analysis of the swimming of microscopic organisms, *Proc. R. Soc. London Ser. A* **209**, 447 (1951).
- [29] P. M. Chaikin and T. C. Lubensky, *Principles of Condensed Matter Physics* (Cambridge University Press, Cambridge, 1995).
- [30] G. Grinstein and R. A. Pelcovits, Nonlinear elastic theory of smectic liquid crystals, *Phys. Rev. A* **26**, 915 (1982).
- [31] P. C. Martin, O. Parodi, and P. S. Pershan, Unified hydrodynamic theory for crystals, liquid crystals, and normal fluids, *Phys. Rev. A* **6**, 2401 (1972).
- [32] G. Volovik and E. Kats, Nonlinear hydrodynamics of liquid crystals, *Sov. Phys. JETP* **54**, 122 (1981).

- [33] W. Helfrich, Capillary Flow of Cholesteric and Smectic Liquid Crystals, *Phys. Rev. Lett.* **23**, 372 (1969).
- [34] M. Kröger and J. Vermant, The structure and rheology of complex fluids, *Appl. Rheol.* **10**, 110 (2000).
- [35] C. Brennen and H. Winet, Fluid mechanics of propulsion by cilia and flagella, *Annu. Rev. Fluid Mech.* **9**, 339 (1977).
- [36] P. G. DeGennes, Viscous flow in smectic a liquid crystals, *Phys. Fluids* **17**, 1645 (1974).
- [37] D. Collin, J. L. Gallani, and P. Martinoty, Nonconventional hydrodynamics of smectic-A phases of liquid crystals: An experimental study of various compounds with the use of ultrasound, *Phys. Rev. A* **34**, 2255 (1986).
- [38] S. Bhattacharya, B. K. Sarma, and J. B. Ketterson, Critical attenuation and dispersion of longitudinal ultrasound near a nematic–smectic-A phase transition, *Phys. Rev. B* **23**, 2397 (1981).
- [39] N. A. Clark, Pretransitional mechanical effects in a smectic-A liquid crystal, *Phys. Rev. A* **14**, 1551 (1976).
- [40] Z. Dogic and S. Fraden, Ordered phases of filamentous viruses, *Curr. Opin. Colloid Interface Sci.* **11**, 47 (2006).